Flagellum inheritance in *Trypanosoma brucei* requires a kinetoplastid-specific protein phosphatase

Received for publication, January 25, 2018, and in revised form, April 16, 2018 Published, Papers in Press, April 17, 2018, DOI 10.1074/jbc.RA118.002106

Qing Zhou[‡], **Gang Dong**[§], **and Ziyin Li**[‡1]

From the [‡]*Department of Microbiology and Molecular Genetics, McGovern Medical School, University of Texas Health Science Center at Houston, Houston, Texas 77030 and the* [§]*Max F. Perutz Laboratories, Vienna Bio-center, Medical University of Vienna, Dr. Bohr-Gasse 9, 1030 Vienna, Austria*

Edited by Ronald C. Wek

Trypanosoma brucei **causes sleeping sickness in humans and nagana in cattle in sub-Saharan Africa and alternates between its mammalian hosts and its insect vector, the tsetse fly.** ***T. brucei*** **uses a flagellum for motility, cell division, and cell– cell communication. Proper positioning and attachment of the newly assembled flagellum rely on the faithful duplication and segregation of flagellum-associated cytoskeletal structures. These processes are regulated by the polo-like kinase homolog TbPLK, whose activity and abundance are under stringent control to ensure spatiotemporally regulated phosphorylation of its substrates. However, it remains unclear whether a protein phosphatase that counteracts TbPLK activity is also involved in this regulation. Here, we report that a putative kinetoplastid-specific protein phosphatase, named KPP1, has essential roles in regulating flagellum positioning and attachment in** ***T. brucei*****. KPP1 localized to multiple flagellum-associated cytoskeletal structures and co-localized with TbPLK in several cytoskeletal structures at different cell-cycle stages. KPP1 depletion abolished basal body segregation, inhibited the duplication of the centrin arm and the hook complex of the bilobe structure, and disrupted the elongation of the flagellum attachment zone, leading to flagellum misplacement and detachment and cytokinesis arrest. Importantly, KPP1-depleted cells lacked dephosphorylation of TbCentrin2, a TbPLK substrate, at late cell-cycle stages. Together, these results suggest that KPP1-mediated protein dephosphorylation regulates the duplication and segregation of flagellum-associated cytoskeletal structures, thereby promoting flagellum positioning and attachment. These findings highlight the requirement of reversible protein phosphorylation, mediated by TbPLK and KPP1, in regulating flagellum inheritance in** ***T. brucei*****.**

Trypanosoma brucei, the causative agent of sleeping sickness in humans and nagana in cattle in sub-Saharan Africa, alternates between the mammalian hosts and the insect vector tsetse fly. The parasite possesses a motile flagellum, which is nucleated from the mature basal body (mBB),[2] exits the cell from the flagellar pocket (FP), and attaches, along most of its length, to the cell body through a specialized cytoskeletal structure termed flagellum attachment zone (FAZ) (1). During the early cell cycle, a new flagellum is nucleated from the newly matured basal body, undergoes a rotational movement toward the posterior side of the old flagellum, and further extends toward the anterior portion of cell with its distal tip tethered to the old flagellum through a motile structure termed flagella connector (2). Consequently, elongation of the new flagellum pushes its associated cytoskeletal structures, including the basal body, the bilobe structure consisting of the hook complex and the centrin arm (3), and the flagellar pocket, toward the cell posterior. Upon cell division, the cleavage furrow assembled between the new and old flagella bisects the cell to produce two daughter cells, each of which inherits one flagellum and its associated cytoskeletal structures. Besides its roles in cell motility, the flagellum also determines cell morphology (4), defines the cell division plane (4), and mediates cell-cell communications (5, 6).

Proper positioning and attachment of the newly synthesized flagellum depend on the duplication and segregation of flagellum-associated cytoskeletal structures (7–12), and are regulated by the polo-like kinase homolog TbPLK, which has a dynamic localization on various flagellum-associated cytoskeletal structures at different cell-cycle stages (13–15). TbPLK appears to function as a master orchestrator of flagellum inheritance in *T. brucei*, as depletion of TbPLK disrupts the duplication and segregation of the cytoskeletal structures that position and attach the flagellum (15). TbPLK may execute this function through regulating its substrates that localize to distinct cytoskeletal structures. SPBB1, a TbPLK substrate in the basal body and previously known as p110 (16), regulates basal body segregation and is required for positioning the flagellum and main-

This work was supported by National Institutes of Health R01 Grants AI101437 and AI118736 (to Z. L.). The authors declare that they have no conflicts of interest with the contents of this article. The content is solely the responsibility of the authors and does not necessarily represent the official views of the National Institutes of Health.
This article contains Figs. S1 and S2.

[1] To whom correspondence should be addressed. Tel.: 713-500-5139; Fax: 713-500-5499; E-mail: Ziyin.Li@uth.tmc.edu.

[2] The abbreviations used are: mBB, mature basal body; kPPP, kinetoplastid-specific phosphoprotein phosphatase; PLK, polo-like kinase; TbPLK, *Trypanosoma brucei* PLK homolog; CIF1, cytokinesis initiation factor 1; SPBB1, substrate of TbPLK in the basal body; PPP, phosphoprotein phosphatase; FAZ, flagellum attachment zone; snFAZ, short new FAZ; FPC, flagellar pocket collar; FP, flagellar pocket; pBB, pro-basal body; CA, centrin arm; HC, hook complex; N, nucleus; K, kinetoplast; PP1, protein phosphatase 1; KPP1, kinetoplastid-specific protein phosphatase 1; NF, new flagellum; OF, old flagellum; MYPT1, myosin phosphatase-targeting subunit 1; PFR2, paraflagellar rod 2; PP2A, protein phosphatase 2A; PAC, puromycin resistance gene; FITC, fluorescein isothiocyanate; HA, hemagglutinin; DAPI, 4′,6-diamidino-2-phenylindole.

taining flagellum attachment to the cell body (8). TbCentrin2, a TbPLK substrate in the centrin arm (17), promotes bilobe duplication (3). Phosphorylation of TbCentrin2 at Ser-54 by TbPLK is important for FAZ elongation and flagellum attachment, but dephosphorylation of TbCentrin2 at Ser-54 is necessary for FAZ elongation and flagellum attachment (17), indicating that an unidentified protein phosphatase is involved in dephosphorylating TbCentrin2. TbPLK itself is under tight control, as excess TbPLK also abolishes basal body segregation and FAZ elongation (18, 19), in part through constitutively phosphorylating TbCentrin2 in the centrin arm (19).

Reversible protein phosphorylation plays crucial roles in regulating many cellular processes in eukaryotes, and requires a protein kinase and an antagonizing protein phosphatase (20). In humans, the function of the polo-like kinase homolog Plk1 is antagonized by myosin phosphatase-targeting subunit 1 (MYPT1)-regulated protein phosphatase 1 catalytic subunit isoform β (PP1Cβ) at the centrosomes (21) and by B56-regulated protein phosphatase 2A (PP2A) at the kinetochores (22). MYPT1-PP1Cβ dephosphorylates Thr-210 in the T-loop of Plk1 to inactivate Plk1 at the centrosomes (21), whereas B56-PP2A dephosphorylates Plk1 substrates to counteract Plk1 function at the kinetochores (22). TbPLK is also activated by phosphorylation of Thr-198, which is analogous to Thr-210 in Plk1, in its T-loop (16), but neither the protein kinase responsible for Thr-198 phosphorylation nor the protein phosphatase responsible for Thr-198 dephosphorylation have been identified. It is also unclear whether any protein phosphatase in *T. brucei* antagonizes TbPLK function by dephosphorylating TbPLK substrates, but the requirement for TbCentrin2 dephosphorylation in the mitotic phase (17) suggests the involvement of an unidentified protein phosphatase.

Here we report that a putative kinetoplastid-specific protein phosphatase co-localizes with TbPLK in different flagellum-associated cytoskeletal structures and regulates the duplication and segregation of these cytoskeletal structures, thereby promoting flagellum positioning and adhesion. These findings highlight the involvement of reversible protein phosphorylation in flagellum inheritance in *T. brucei*.

Results

KPP1 co-localizes with TbPLK at several flagellum-associated cytoskeletal structures

A putative serine/threonine protein phosphatase, encoded by Tb927.5.4380, was previously identified as a near neighbor of CIF1 (23), suggesting that it may localize to the new FAZ tip and plays roles in cytokinesis initiation. It was previously annotated as a kinetoplastid-specific phosphoprotein phosphatase (kPPP) (24). Bioinformatics analysis and homology modeling by SWISS-MODEL (25) revealed an N-terminal domain, which is structurally similar to the Plus3 domain in human RNA polymerase II-associated RTF1 (Fig. 1, *A–C*), and a C-terminal phosphatase catalytic domain, which exhibits ~28/60% sequence identity/similarity to the human protein phosphatase 1 catalytic subunit isoform γ (PP1Cγ) (Fig. 1, *A*, *D*, and *E*, and Fig. S1) and the eight PP1 homologs and two PP2A homologs from *T. brucei* (Fig. S1). Given its unusual N-terminal Plus3 domain, the C-terminal protein phosphatase catalytic domain, and the presence of close homologs in other kinetoplastid parasites (Figs. S1 and S2), we named this protein KPP1 for Kinetoplastid-specific Protein Phosphatase 1. The Plus3 domain in human RTF1 consists of six α helices intervened by six β sheets in a mixed α/β-fold (26), and is involved in binding to a phosphothreonine-containing repeat sequence of the transcription elongation factor Spt5 (27). Notably, four of the five residues in the RTF1 Plus3 domain that are involved in direct binding to the phosphothreonine residue of Spt5 are also found in the Plus3 domain of KPP1 (Fig. 1*B*, *blue arrowheads*). Therefore, the Plus3 domain in KPP1 may be similarly involved in binding to phosphothreonine-containing proteins in *T. brucei*.

The modeled catalytic domain of KPP1 adopts a structure composed of an α/β-fold, with a β sandwich situated between two α-helical domains (Fig. 1*D*), similar to that of the human PP1Cγ (Fig. 1*E*) and other PP1 catalytic subunit proteins (28). It possesses all six conserved residues (Asp-336, His-338, Asp-371, Asn-403, His-462, and His-557) in the catalytic site (Fig. S1, *green boxes*) to coordinate two manganese ions, which are located at the three-way joint of the two α-helical domains and the β sandwich (Fig. 1, *E* and *F*).

KPP1 was endogenously tagged with a triple HA epitope and its subcellular localization during the cell cycle was determined by immunofluorescence microscopy. At G_1 phase, KPP1 localizes to the basal body and the centrin arm, which were labeled with the anti-LdCen1 antibody that detects centrins at the basal body and the centrin arm, and co-localizes with TbPLK at both structures (Fig. 2, *A* and *B*). From S phase to mitotic phases, KPP1 localizes to the duplicated basal bodies, the duplicated centrin arms, and the new FAZ tip (Fig. 2, *A*, *C*, and *D*) and co-localizes with TbPLK at the new FAZ tip (Fig. 2*A*). FAZ was labeled with the anti-CC2D antibody, and basal body was labeled with the anti-TbSAS-6 antibody. In post-mitotic cells during which TbPLK disappears from the new FAZ tip, KPP1 also disappears from the new FAZ tip, but it remains in the basal bodies and the centrin arms (Fig. 2*A*). Given that the KPP1 fluorescence signal at the new FAZ tip in mitotic cells is much weaker than in pre-mitotic cells (Fig. 2, *A* and *D*), it suggests that starting from mitotic phases KPP1 gradually disappears from the new FAZ tip. Additionally, KPP1 is also detected at the flagella connector region (Fig. 2, *A* and *C*), where it co-localizes with TbPLK (Fig. 2*A*). Moreover, KPP1 is also detected as some weaker punctate dots in the cytosol (Fig. 2), suggesting the distribution of KPP1 in some cytosolic compartments.

We also investigated whether mutation of the active sites in the catalytic domain of KPP1 affects KPP1 localization. Immunofluorescence microscopy showed that ectopically expressed WT KPP1, which was tagged with a C-terminal triple HA epitope, displayed normal localization patterns (Fig. 2*E*). However, ectopically expressed mutant KPP1 that bore point mutations at two of the six conserved active sites (D371N and H557K) localized to the cytosol (Fig. 2*E*), indicating that the activity of KPP1 is required for KPP1 localization. Altogether, the localization of KPP1 to various flagellum-associated cytoskeletal structures indicates that KPP1 may play roles in the duplication and/or segregation of these cytoskeletal structures.

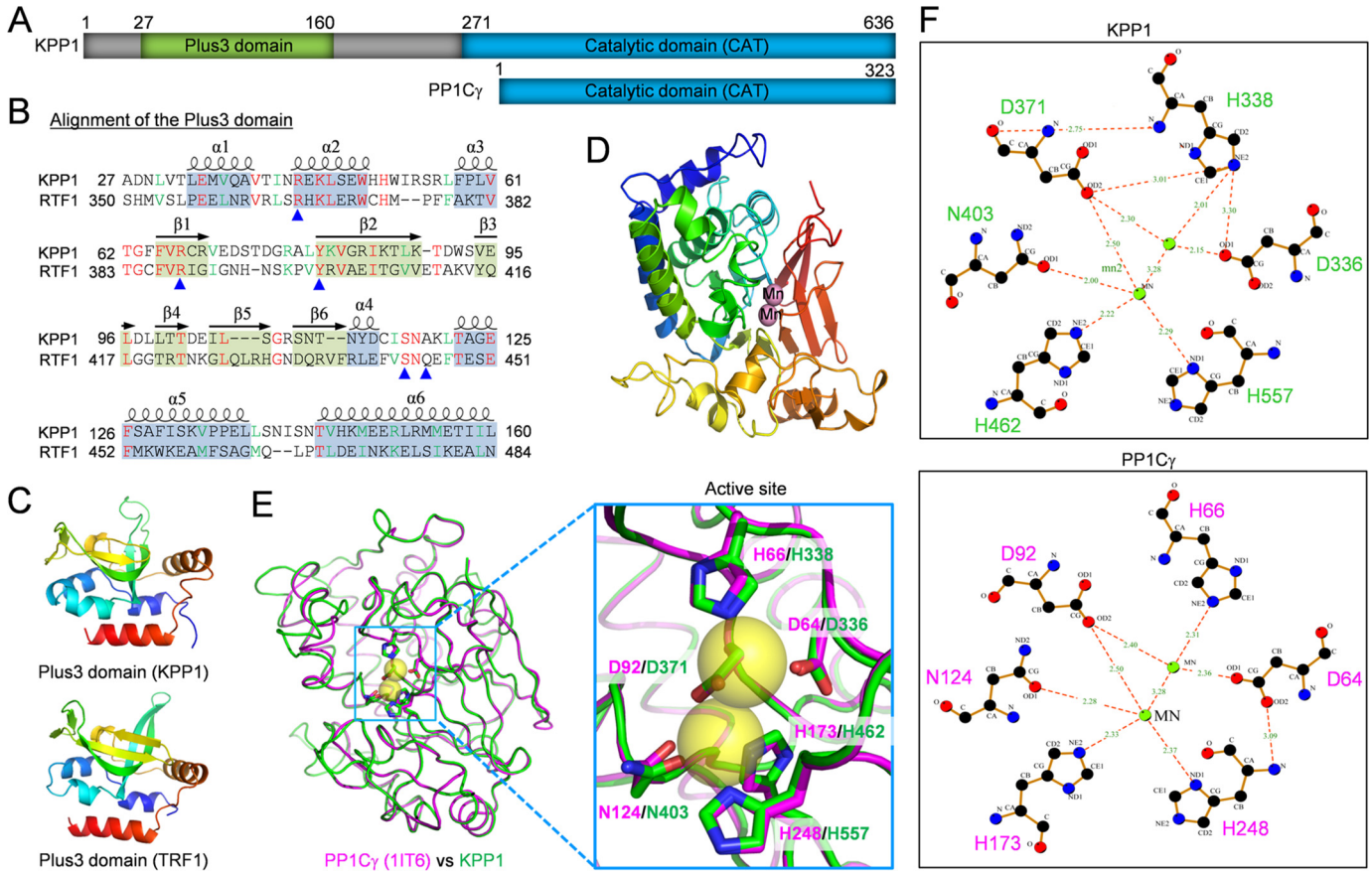

Figure 1. KPP1 is a kinetoplastid-specific protein phosphatase PP1 homolog. *A,* schematic illustration of the structural motifs in KPP1 and human serine/threonine protein phosphatase PP1 catalytic subunit isoform γ (PP1Cγ). *B,* sequence alignment of the Plus3 domain of KPP1 and human RTF1. The α helices and β sheets are based on the structure of RTF1 Plus3 domain. *Blue arrowheads* indicate the residues involved in direct binding to the phosphothreonine residue of RTF1-interacting protein Spt5. *C,* modeling of the Plus3 domain of KPP1 by SWISS MODEL using the template 4L1P (Plus3 domain of RTF1). *D,* modeling of the catalytic domain of KPP1 by SWISS MODEL. The template used is 1IT6 (PP1Cγ). The two bound manganese ions (Mn) are shown as *spheres*. *E,* superimposition of the modeled KPP1 catalytic domain onto the human PP1Cγ crystal structure. *Yellow spheres* indicate the manganese ions located in the active site. The six manganese-coordinating residues are indicated in the enlarged structure. *F,* comparison of the active site and the six manganese-coordinating residues between KPP1 and human PP1Cγ. The distance from the manganese ions to each of the six amino acids is shown in Angstroms.

KPP1 is essential for FAZ elongation and flagellum attachment

The physiological function of KPP1 was investigated by RNAi in the procyclic form of *T. brucei*. Western blotting confirmed the knockdown of KPP1 protein, which was endogenously tagged with a triple HA epitope, after 24 h of RNAi induction (Fig. 3*A*). KPP1-depleted cells had a growth rate similar to the noninduced control cells up to 48 h of RNAi induction, but stopped growing thereafter (Fig. 3*B*), suggesting that KPP1 is essential for cell proliferation. Quantitation of the cells containing different numbers of nuclei and kinetoplasts showed that starting from 72 h of RNAi induction, cells with one nucleus and one kinetoplast (1N1K) decreased to ~15% of the total population, and cells with more than two nuclei increased to ~67% of the total population after 96 h of RNAi (Fig. 3*C*), suggesting defective cytokinesis. Moreover, anucleated zoid cells (0N1K) and cells with two nuclei and one kinetoplast (2N1K) also emerged (Fig. 3*C*), indicating that aberrant cytokinesis occurred in some cells. The 2N1K cells could also be derived from 1N1K cells in the absence of kinetoplast segregation but normal mitosis.

The most notable phenotype caused by KPP1 depletion is flagellum detachment in ~60% of the total cell population after 72 h of RNAi induction (Fig. 3*D*). Flagellum detachment was observed in almost all cell types (Fig. 3*E*). To investigate whether flagellum detachment is due to the defects in FAZ assembly/elongation, cells were immunostained with anti-FAZ1 antibody, and the number of FAZ was tabulated (Fig. 3, *E* and *F*). The results showed that the 1N1K cells with one FAZ were significantly increased after KPP1 RNAi, which was accompanied by a significant decrease of the cells with two FAZs (Fig. 3, *E* and *F*). Similarly, the 1N2K and 2N2K cells with only one FAZ or with one short new FAZ (snFAZ) and one normal old FAZ emerged to more than 60% for each cell type, and consequently, the cells with two FAZs were significantly decreased after KPP1 RNAi (Fig. 3, *E* and *F*). Strikingly, ~94% of the 2N1K cells from the KPP1 RNAi cells contained either one normal old FAZ or one snFAZ and one normal old FAZ (Fig. 3, *E* and *F*). These results demonstrated that assembly/elongation of the new FAZ was disrupted by KPP1 depletion, thus leading to flagellum detachment.

KPP1 is required for proper positioning of the new flagellum

The flagellum was immunostained with L8C4 (anti-PFR2) antibody, which detects the paraflagellar rod 2 (PFR2) protein

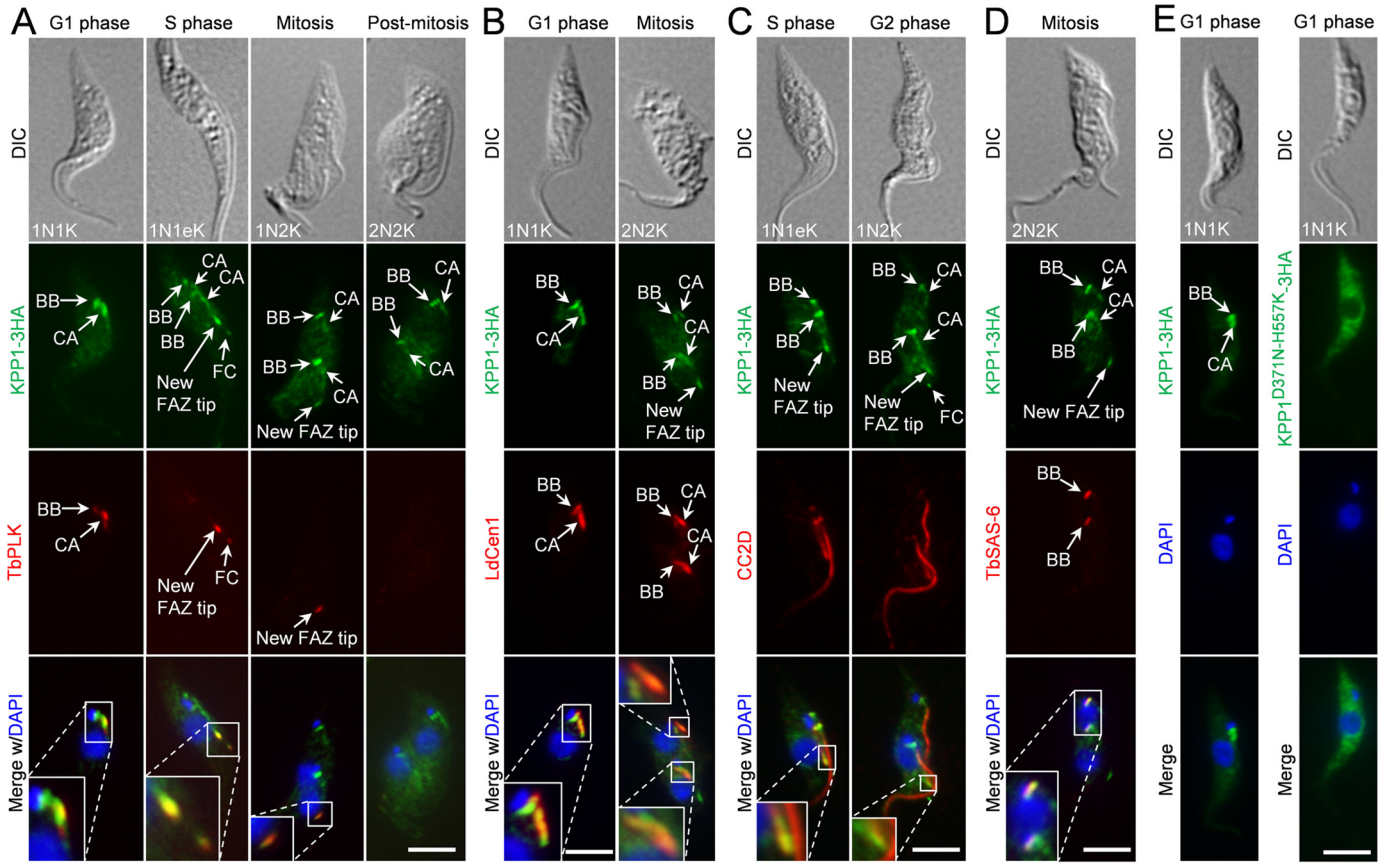

Figure 2. KPP1 localizes to multiple flagellum-associated structures and co-localizes with TbPLK at the basal body, the centrin arm, and the new FAZ tip. *A,* subcellular localization of KPP1 during the cell cycle and co-localization of KPP1 with TbPLK. KPP1 was endogenously tagged with a triple HA epitope and detected by FITC-conjugated anti-HA mAb, whereas TbPLK was detected by anti-TbPLK pAb. Cells were counterstained by DAPI for nuclear and kinetoplast DNA. *BB*, basal body; *CA*, centrin arm; *FC*, flagella connector. *Scale bar*, 5 μm. *B,* KPP1 localizes to the basal body and the centrin arm. Shown are the co-immunostaining of cells with FITC-conjugated anti-HA mAb to detect KPP1–3HA and anti-LdCen1 pAb to label the basal body and the centrin arm. *Scale bar*, 5 μm. *C* and *D,* KPP1 localizes to the new FAZ tip and the basal body. Shown in *C* are an S-phase cell and a G_2 cell co-immunostained with FITC-conjugated anti-HA mAb to detect KPP1–3HA and anti-CC2D pAb to label the FAZ, and shown in *D* is a mitotic cell co-immunostained with FITC-conjugated anti-HA mAb to detect KPP1–3HA and anti-TbSAS6 pAb to label the basal body. *E*, localization of triple HA-tagged wild-type KPP1 and a mutant KPP1 bearing two point mutations in the active sites. Cells were immunostained with FITC-conjugated anti-HA mAb and counterstained with DAPI. *Scale bars*, 5 μm.

in the flagellum (Fig. 4*A*), and was tabulated in control and KPP1 RNAi cells. The results showed that formation of the new flagellum was not affected by KPP1 depletion, as the 1N1K cells with two flagella slightly increased and the majority of the 1N2K, 2N2K, and 2N1K cells had two flagella (Fig. 4*B*). However, the location of the newly assembled flagellum in the bi-flagellated 1N1K, 1N2K, 2N2K, and 2N1K cells collected from KPP1 RNAi-induced cell population was very close to that of the old flagellum (Fig. 4*A*, *KPP1 RNAi*), in striking contrast to the bi-flagellated control cells in which the new flagellum was separated from the old flagellum and moved toward the cell posterior (Fig. 4*A*, *Control*). These results suggest that positioning of the new flagellum was compromised by KPP1 depletion.

RNAi of KPP1 impairs basal body segregation

The emergence of 2N1K cells after KPP1 RNAi (Fig. 3*C*) suggests that kinetoplast segregation is likely impaired. Because kinetoplast segregation is mediated by basal body segregation (29), it suggests that KPP1 RNAi may inhibit basal body duplication and/or segregation. Therefore, we investigated the effect of KPP1 depletion on basal body duplication and/or segregation. Quantitation of the mBB, which was labeled by the YL 1/2 antibody, showed that after KPP1 RNAi, the 1N1K cells with two mBBs increased, and the 1N2K and 2N2K cells with two or more than two mBBs were slightly, but not significantly, decreased (Fig. 4*B*), suggesting that basal body duplication was not compromised. Co-immunostaining of the KPP1 RNAi cells with the anti-TbSAS6 antibody, which labels the cartwheel structure of both the mBB and the pro-basal body (pBB), and the YL 1/2 antibody showed that all the 2mBB-containing cells also possess two pro-basal bodies, *i.e.* 2mBB-2pBB (Fig. 4*C*), further confirming that basal body duplication was not affected by KPP1 RNAi. Notably, in the 1N2K, 2N2K, and 2N1K cells, but not the 1N1eK cells with an elongated kinetoplast, the distance between the two pairs of mBB–pBB in KPP1 RNAi cells was significantly shorter than that in the control cells (Fig. 4, *A*, *C*, and *D*), suggesting defective basal body segregation.

The 2N1K cells could also be generated if aberrant cytokinesis occurs in 2N2K cells, which also produces zoid (0N1K) cells that contain a flagellum and a pair of mBB–pBB. KPP1 RNAi did produce ~6% zoid cells (Fig. 3*C*), but it should be noted that ~70% of the 2N1K cells from KPP1 RNAi contained two flagella and two pairs of mBB–pBB (Fig. 4, *B* and *C*), suggesting

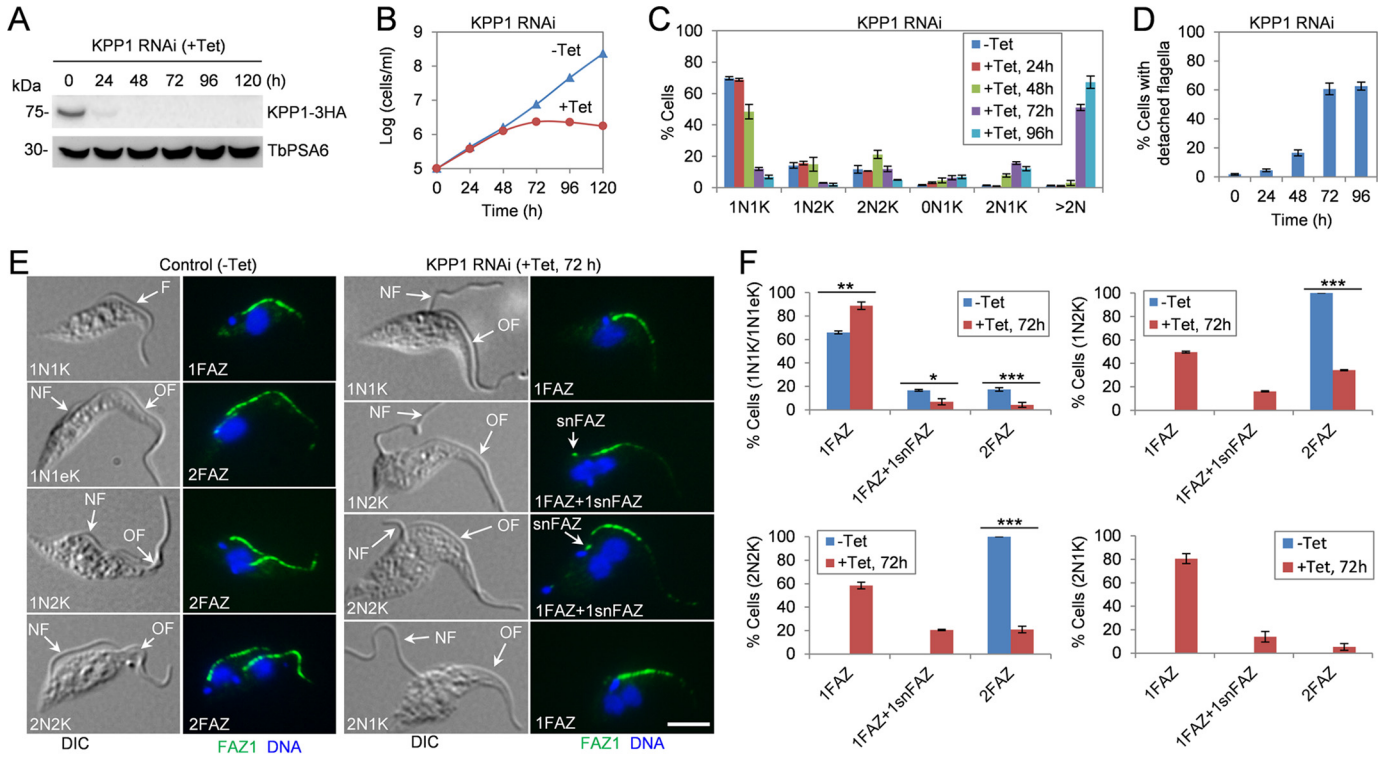

Figure 3. KPP1 is essential for FAZ elongation and flagellum attachment. *A,* Western blotting to monitor the level of KPP1 protein before and after KPP1 RNAi induction. KPP1 was endogenously tagged with a triple HA epitope and detected by anti-HA antibody. TbPSA6 serves as the loading control. *B,* KPP1 depletion caused a severe growth defect. *C,* effect of KPP1 depletion on cell-cycle progression. Shown is the quantitation of control cells (−*Tet*) and KPP1 RNAi-induced cells (+*Tet*) at different cell-cycle stages. 200 cells at each time point were collected by centrifugation, fixed with paraformaldehyde, stained with DAPI, and counted for the numbers of nucleus and kinetoplast. Three independent repeats were conducted. *Error bars* indicate S.D. *D,* KPP1 depletion caused flagellum detachment. Shown is the quantitation of cells with a detached flagellum in noninduced control cells (0 h) and KPP1 RNAi cells that were induced for up to 96 h. A total of 100 cells were counted for each time point, and three repeats were carried out. *Error bars* indicate S.D. *E,* immunostaining of control cells and KPP1 RNAi cells with the anti-FAZ1 mAb to label the FAZ. *NF*, new flagellum; *OF*, old flagellum. *Scale bar*, 5 μm. *F,* quantitation of the FAZ in control cells (−*Tet*) and KPP1 RNAi cells (+*Tet*) that were induced for 72 h. A total of 100 cells for each cell type (1N1K/1N1eK, 1N2K, 2N2K, and 2N1K) were counted, and three repeats were conducted. *Error bars* indicate S.D. *, $p < 0.05$; **, $p < 0.01$; ***, $p < 0.001$.

that they were not generated through aberrant cytokinesis of 2N2K cells. Rather, these 2N1K cells were produced due to failed basal body segregation, which is known to inhibit kinetoplast segregation (29). Collectively, these results suggest that KPP1 depletion impaired the segregation, but not duplication, of basal bodies.

KPP1 is necessary for duplication and segregation of the flagellar pocket collar

The defective positioning of the new flagellum in KPP1 RNAi cells (Fig. 4*A*) suggests that biogenesis and/or segregation of the flagellar pocket collar (FPC) may also be compromised. To test this possibility, we immunostained the cells with anti-BILBO1 antibody to label the FPC (Fig. 5*A*) and counted the numbers of FPC in control and KPP1 RNAi cells (Fig. 5*B*). The results showed that in the three cell types (1N1K, 1N2K, and 2N2K) examined, the cells with two FPC were significantly decreased, accompanied by a corresponding increase of 1N1K cells with one FPC and emergence of 1N2K and 2N2K cells with one FPC (Fig. 5*B*). In the 2N1K cells from the KPP1 RNAi population, ~65% contained only one FPC (Fig. 5, *A* and *B*). These results suggest that FPC duplication was impaired in KPP1 RNAi cells. We further measured the inter-FPC distance in cells containing two FPCs, and the results showed that the average inter-FPC distance in 2N2K and 2N1K cells was significantly decreased upon KPP1 RNAi (Fig. 5*C*), indicating that in these cells the duplicated FPCs failed to segregate. Scanning electron microscopy confirmed that the bi-flagellated KPP1 RNAi cells contained either only one flagellar pocket from which both flagella exited the cell body (Fig. 5*D*, *panel b*) or two closely associated flagellar pockets (Fig. 5*D*, *panels c* and *d*). Together, these results suggest that KPP1 depletion disrupted the duplication and segregation of the flagellar pocket.

KPP1 is essential for the duplication of the centrin arm and the hook complex of the bilobe structure

The previously described bilobe structure (3) contains a centrin arm, which is marked by TbCentrin2 and TbCentrin4 (3, 30), and a hook complex, which is marked by TbMORN1 (31). The localization of KPP1 to the centrin arm of the bilobe (Fig. 2*B*) suggests its potential role in bilobe duplication and/or segregation. To test this possibility, cells were co-immunostained with the pan-centrin antibody 20H5 to label the centrin arm and the anti-TbMORN1 antibody to label the hook complex, and the numbers of centrin arm and hook complex were counted and compared between the control and KPP1 RNAi cells. In the 1N1K, 1N2K, and 2N2K cells examined, those cells with one centrin arm and one hook complex were significantly increased after KPP1 RNAi, which was accompanied by a corresponding decrease of the cells with two centrin arms and two

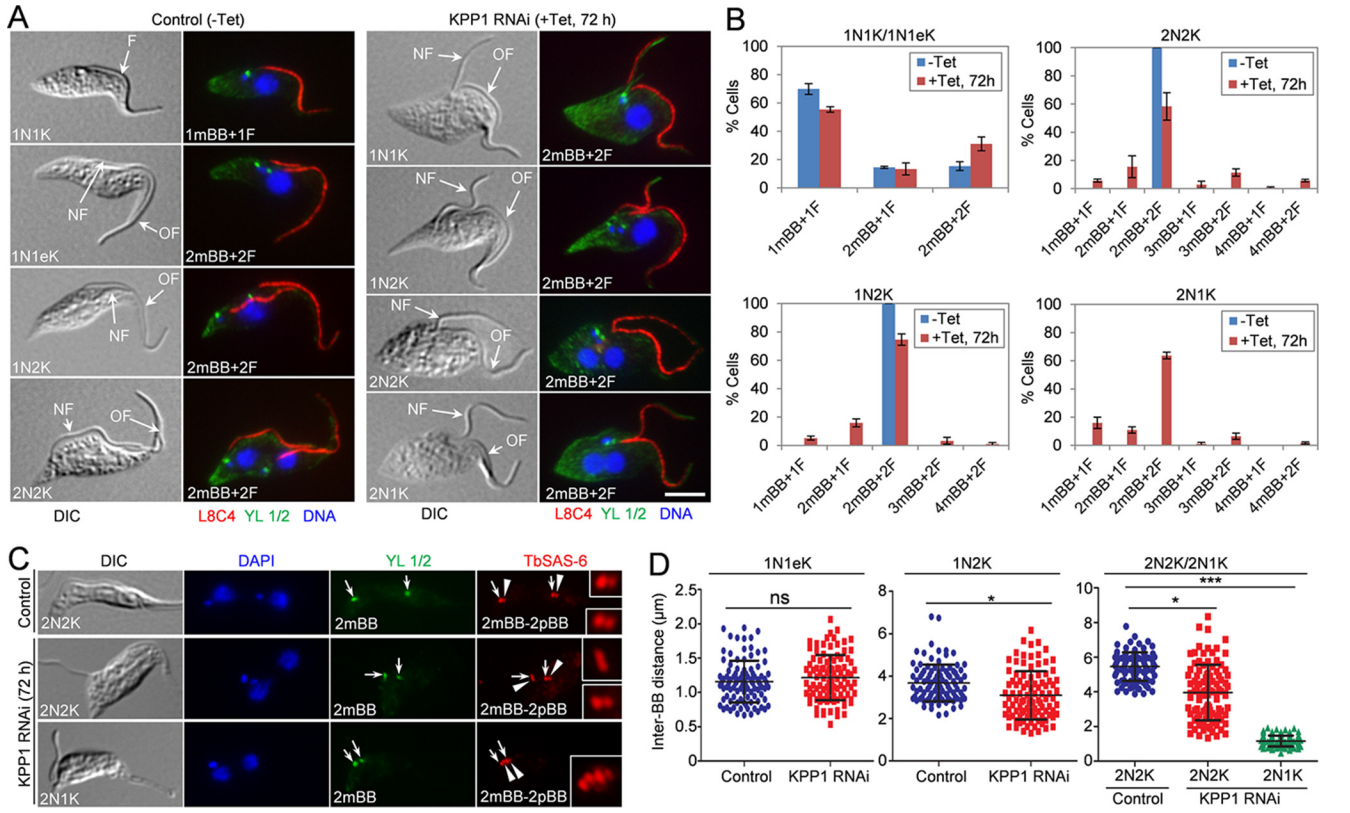

Figure 4. KPP1 is required for segregation of the duplicated basal bodies and flagella. *A,* co-immunostaining of cells with the L8C4 antibody to label the flagellum (*F*) and the YL 1/2 antibody to label the flagellum-associated mBB. *NF*, new flagellum; *OF*, old flagellum. *Scale bar*, 5 μm. *B,* quantitation of the flagellum and the mature basal body in control cells (−*Tet*) and KPP1 RNAi cells (+*Tet*) that were induced for 72 h. 200 cells of each cell type (1N1K/1N1eK, 1N2K, 2N2K, and 2N1K) were counted, and three repeats were conducted. *Error bars* indicate S.D. *C,* co-immunostaining of cells with the YL 1/2 antibody to label mBB and the anti-TbSAS-6 antibody to label both the mBB (*arrows*) and pBB (*arrowheads*). *Scale bar*, 5 μm. *D,* measurement of inter-basal body (*BB*) distance in control and KPP1 RNAi cells. The 1N1eK cells are S-phase cells containing an elongated kDNA and duplicated basal bodies (*2mBB–2pBB*). The inter-BB distance was defined by the distance between the two mBB–pBB pairs. A total of 100 cells of each cell type were used for measurement with the ImageJ software. *ns*, no statistical significance; *, $p < 0.05$; ***, $p < 0.001$.

hook complexes (Fig. 6, *A* and *B*). Similarly, the majority (~80%) of the 2N1K cells in the KPP1 RNAi cell population contained one centrin arm and one hook complex (Fig. 6, *A* and *B*). These results indicate that KPP1 depletion impaired duplication of both the centrin arm and the hook complex in the bilobe structure.

Depletion of KPP1 abolishes dephosphorylation of TbCentrin2 in mitotic cells

We asked whether KPP1 is likely to counteract TbPLK function by dephosphorylating TbPLK substrate(s). So far only two TbPLK substrates, TbCentrin2 (14, 17) and SPBB1 (8), have been experimentally validated, and TbPLK phosphorylation of TbCentrin2 can be detected by the PS54 antibody, which was raised against the TbPLK-phosphorylated Ser-54 of TbCentrin2 (17). Using the PS54 antibody, we assessed the effect of KPP1 depletion on TbCentrin2 phosphorylation. In the noninduced control cells, PS54 detects phospho-TbCentrin2 at the centrin arm in ~45% of the 1N1K and 1N1eK cells (Fig. 7*A*). In ~56% of 1N2K cells, phospho-TbCentrin2 is still detectable in the two segregated centrin arms, but the signal becomes much weaker (Fig. 7*A*). In all of the 2N2K cells, the PS54 signal is undetectable (Fig. 7*A*), suggesting that TbCentrin2 is dephosphorylated in mitotic cells. Knockdown of TbPLK completely eliminated PS54 staining (Fig. 7*B*), confirming that Ser-54 is a site phosphorylated by TbPLK. In KPP1 RNAi cells, PS54 detects phospho-TbCentrin2 in ~41% of the 1N1K and 1N1eK cells and ~53% of the 1N2K cells (Fig. 7, *C* and *D*), similar to that in the control cells. However, PS54 signal is still detectable in the centrin arms in ~63% of the bi-nucleated cells (2N2K and 2N1K) (Fig. 7, *C* and *D*), suggesting that TbCentrin2 was not dephosphorylated during the mitotic phase in KPP1 RNAi cells. The phospho-TbCentrin2 detected in these mitotic cells could be attributed to failure in dephosphorylation. These results suggest that KPP1 may antagonize TbPLK function by controlling, either directly or indirectly, TbCentrin2 dephosphorylation after cells enter mitosis.

Knockdown of KPP1 impairs TbPLK localization to the new FAZ tip at late cell-cycle stages

We investigated the effect of KPP1 deficiency on the subcellular localization of TbPLK by immunofluorescence microscopy. In noninduced control cells, TbPLK localized to the basal body and the centrin arm in some 1N1K cells, and to the new FAZ tip in 1N1eK cells (S-phase), 1N2K cells (G_2 to metaphase), and some 2N2K cells that are in the early anaphase stage (Fig. 8, *A* and *B*). It was not detectable in the 2N2K cells that are in late anaphase and telophase (Fig. 8, *A* and *B*). In KPP1 RNAi cells that were induced for 48 h, TbPLK localization to the basal body and the centrin arm in 1N1K cells and to the new FAZ tip in

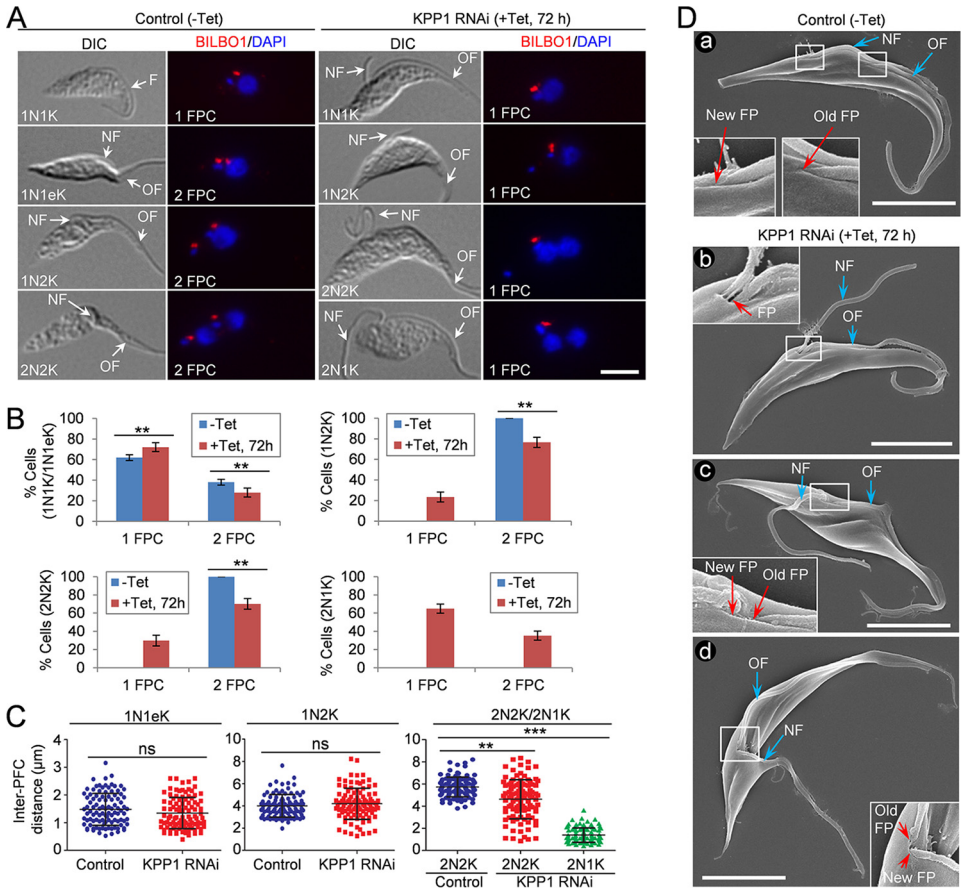

Figure 5. KPP1 is required for duplication and segregation of the flagellar pocket. *A,* immunostaining of control cells (−*Tet*) and KPP1 RNAi cells with the anti-TbBILBO1 antibody to label the flagellar pocket collar (*PFC*). *NF*, new flagellum; *OF*, old flagellum. *Scale bar*, 5 μm. *B,* quantitation of the PFC in control cells (−*Tet*) and KPP1 RNAi cells. 200 cells for each cell type (1N1K/1N1eK, 1N2K, and 2N2K) were counted, and three repeats were conducted. *Error bars* indicate S.D. **, $p < 0.01$. *C,* measurement of inter-PFC distance in control and KPP1 RNAi cells. The 1N1eK cells are S-phase cells containing an elongated kDNA and two FPCs. A total of 100 cells of each cell type (1N1eK, 1N2K, and 2N2K) were used for measurement with the ImageJ software. *ns*, no statistical significance; **, $p < 0.01$; ***, $p < 0.001$. *D,* scanning electron microscopic images of control and KPP1 RNAi cells, showing the FP, NF, and OF. *Panel a* is a control bi-flagellated cell with two far-segregated flagellar pockets, *panel b* is a KPP1-deficient bi-flagellated cell with a single flagellar pocket containing two flagella, *panel c* is a KPP1-deficient bi-flagellated cell with two closely associated flagellar pockets, and *panel d* is a dividing cell with two closely associated flagellar pockets. *Scale bars*, 5 μm.

1N1eK cells was not affected (Fig. 8, *A* and *B*). However, TbPLK localization to the new FAZ tip in 1N2K and 2N2K cells was significantly impaired, resulting in the increase of cells either with undetectable TbPLK signal (no signal) or with TbPLK detected near the flagellar pocket region (FP region) (Fig. 8, *A* and *B*). These results suggest that KPP1 is required for maintaining TbPLK at the new FAZ tip during G_2 to anaphase.

Discussion

Protein phosphorylation is one of the most important post-translational protein modifications and plays crucial roles in various cellular processes in eukaryotes. The cellular processes that are controlled by protein phosphorylation often are also regulated by an antagonizing protein phosphatase, which dephosphorylates the substrate(s) of the protein kinase or dephosphorylates the protein kinase to inactivate the latter (20). These counteracting actions by protein phosphatases provide a means to fine-tune the protein kinase-mediated signaling cascades required to carry out complex physiological and developmental processes. In humans, Plk1 is antagonized by two different protein phosphatases at different subcellular locations through distinct mechanisms (21, 22). It is counteracted by PP1Cβ through dephosphorylation of pThr-210 of Plk1 at centrosomes (21), and by PP2A through dephosphorylating multiple Plk1 substrates at kinetochores (22). In *T. brucei*, a TbPLK-counteracting protein phosphatase is likely also required, as previous studies demonstrated that dephosphorylation of TbCentrin2, a TbPLK substrate in the centrin arm, is necessary for flagellum positioning and attachment (17) and that TbPLK activity is tightly controlled by phosphorylation/dephosphorylation of two threonine residues (Thr-198 and Thr-202) in its T-loop (16). Our findings that KPP1 co-localizes with TbPLK at multiple cytoskeletal structures (Fig. 2*A*) and that KPP1 depletion abolished the dephosphorylation of TbCentrin2 in mitotic cells (Fig. 7, *B* and *C*) suggest that KPP1 is likely able to antagonize TbPLK function. KPP1 may execute this function through dephosphorylation of phospho–Thr-198 and/or phospho–Thr-202 in the T-loop of TbPLK, as in the case of PP1Cβ-mediated counteraction of Plk1 in humans (21). In such a scenario, KPP1 depletion will cause constitutive activation of TbPLK due to lack of T-loop dephosphorylation, and the constitutively active TbPLK may phosphorylate TbCentrin2 in mitotic cells. Alternatively, KPP1 may dephosphorylate TbPLK

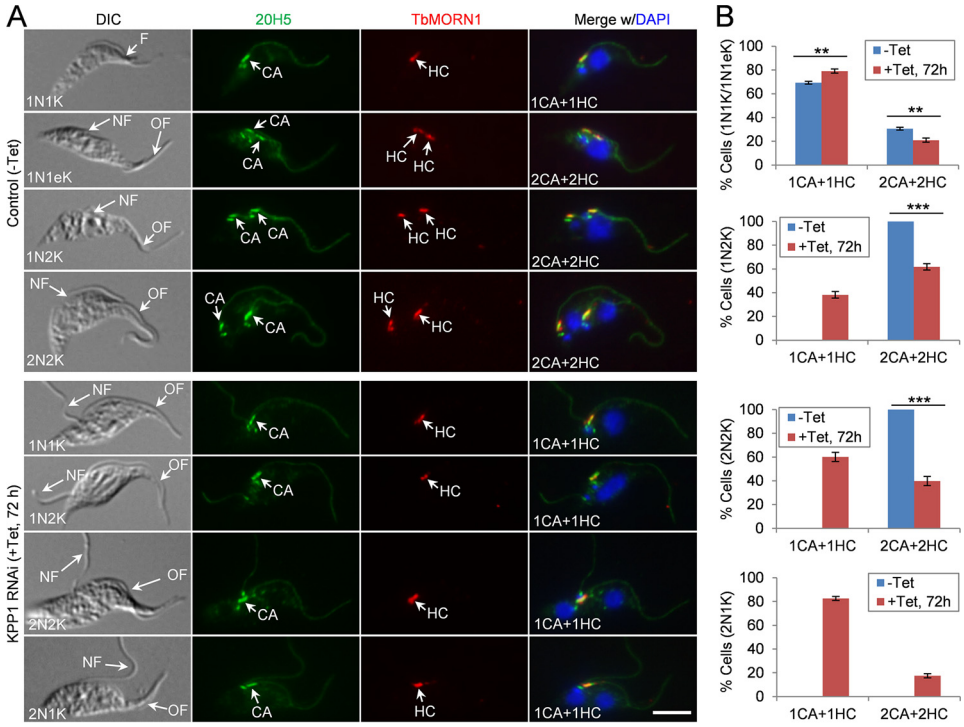

Figure 6. KPP1 is required for duplication of the centrin arm and the hook complex of the bilobe structure. *A*, co-immunostaining of control and KPP1 RNAi cells with the 20H5 mAb, which labels the centrins in the centrin arm (*CA*), and the anti-TbMORN1 pAb, which labels the hook complex (*HC*). *NF*, new flagellum; *OF*, old flagellum. *Scale bar*, 5 μm. *B*, quantitation of the centrin arm and the hook complex in control and KPP1 RNAi cells. A total of 100 cells for each cell type (1N1K/1N1eK, 1N2K, 2N2K, and 2N1K) were counted, and three repeats were conducted. *Error bars* indicate S.D. **, $p < 0.01$. ***, $p < 0.001$.

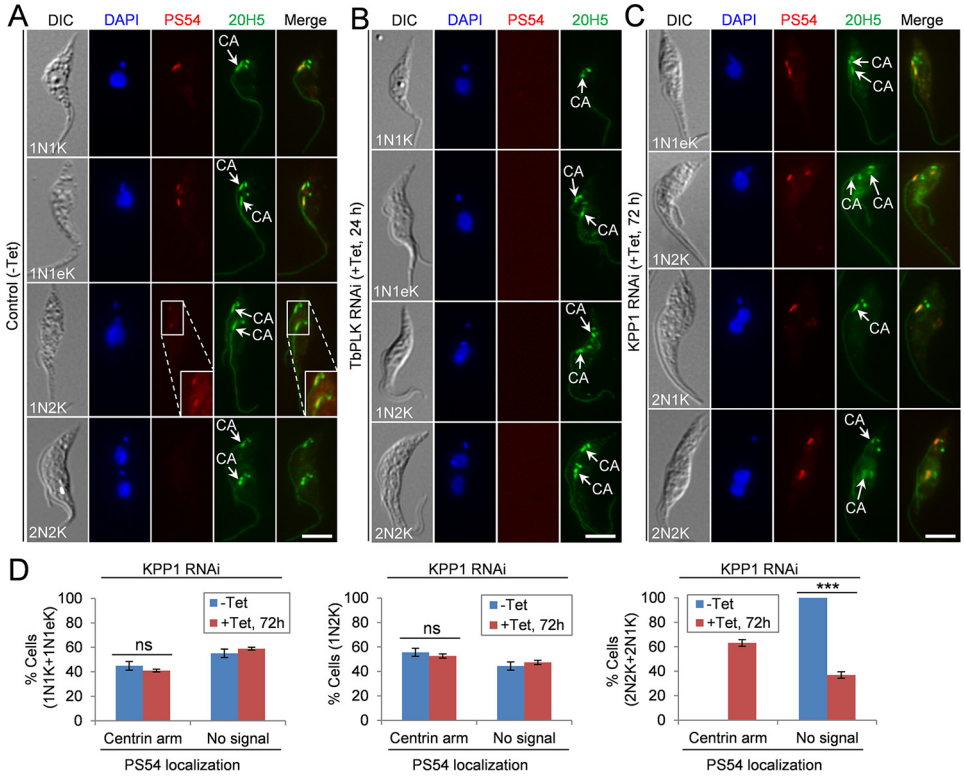

Figure 7. Depletion of KPP1 results in lack of TbCentrin2 dephosphorylation in the centrin arm in mitotic cells. *A–C*, immunostaining of control cells (*A*), TbPLK RNAi cells (*B*), and KPP1 RNAi cells (*C*) with the PS54 antibody, which detects the pSer-54 of TbCentrin2, and the 20H5 antibody, which labels the centrin arm (*CA*) and the basal body (*BB*). The enlarged image in the PS54 channel of the control 1N2K cell shows the longer exposure of the fluorescence signal. *Scale bars*, 5 μm. *D*, quantitation of PS54-positive and PS54-negative cells in control and KPP1 RNAi cells. A total of 100 cells for each cell group (1N1K/1N1eK, 1N2K, and 2N2K/2N1K) were counted, and three repeats were conducted. *Error bars* indicate S.D. ***, $p < 0.001$; *ns*, no statistical significance.

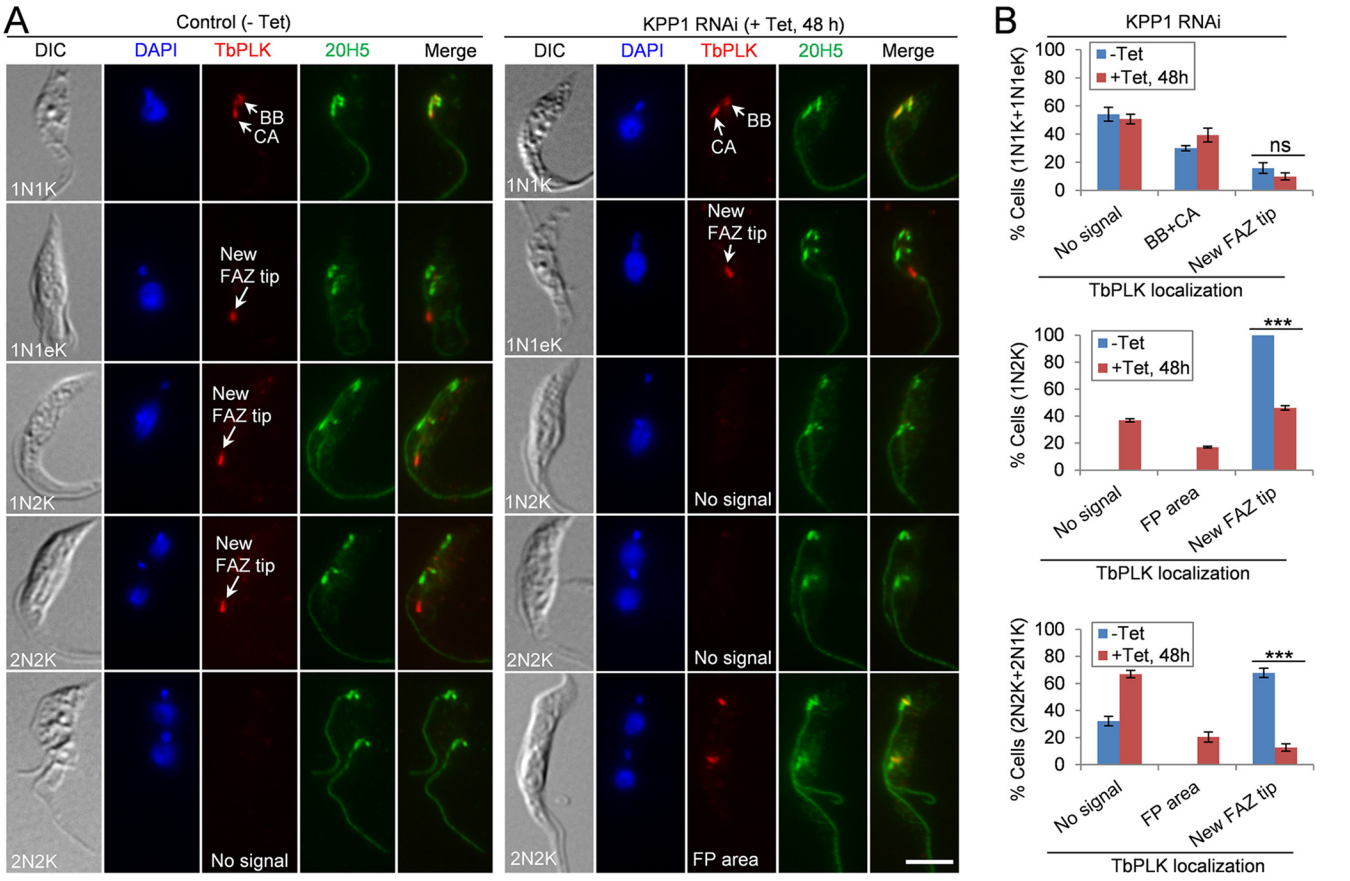

Figure 8. Depletion of KPP1 impairs TbPLK localization to the new FAZ tip during late cell-cycle stages. *A,* immunostaining of control and KPP1 RNAi cells with anti-TbPLK antibody and 20H5 antibody, which labels the centrin arm (*CA*) and the basal body (*BB*). *Scale bar*, 5 μm. *B,* quantitation of TbPLK localization patterns in control and KPP1 RNAi cells. A total of 200 cells for each cell group (1N1K/1N1eK, 1N2K, and 2N2K/2N1K) were counted, and three independent repeats were conducted. *Error bars* indicates S.D. ***, $p < 0.001$; *ns*, no statistical significance.

substrate(s) in the basal body, the centrin arm, or the new FAZ tip, as in the case of PP2A-mediated counteraction of Plk1 in humans (22). In this scenario, KPP1-deficient cells will fail to dephosphorylate TbCentrin2 in mitotic cells. Another possibility is that the mis-localized TbPLK at the flagellar pocket region of the KPP1 RNAi cells (Fig. 8) may continue to phosphorylate TbCentrin2, resulting in the observed phenotype of lack of TbCentrin2 dephosphorylation (Fig. 7). In this scenario, KPP1 dephosphorylates neither TbCentrin2 nor TbPLK, but regulates TbPLK localization through unknown mechanisms. Future efforts will be directed to test these possibilities, which will help ascertain the molecular function of KPP1.

The co-localization of KPP1 with TbPLK at the basal body, the centrin arm, and the new FAZ tip from G_1 phase to early mitosis (Fig. 2*A*) raises an interesting question of how KPP1 counteracts TbPLK function at all these cell-cycle stages. It should be noted that the human Plk1-antagonizing protein phosphatase MYPT1-PP1Cβ also co-localizes with Plk1 at multiple subcellular structures during the cell cycle (21). Previous results showed that TbPLK activity is under tight control during the cell cycle (16, 18), suggesting that TbPLK activity has to be maintained at a certain level at these cell-cycle stages to ensure proper regulation of its substrates. Moreover, previous results also showed that both hypophosphorylation and hyperphosphorylation of TbCentrin2 at Ser-54 caused a growth defect in *T. brucei* (17), suggesting that the phosphorylation level of TbCentrin2 is under tight control. We thus postulate that co-localization of KPP1 with TbPLK at these cell-cycle stages may balance the phosphorylation level of TbPLK and/or its substrates so as to maintain their phosphorylation level within a certain threshold. The level of phosphorylation that is higher or lower than this threshold will cause defects in the positioning and adhesion of the new flagellum.

The *T. brucei* genome encodes a total of 27 phosphoprotein phosphatase (PPP) homologs, including eight PP1 homologs, two PP2A homologs, two PP2B homologs, one PP4 homolog, one PP5 homolog, two PP7 homolog, and 11 kinetoplastid-specific PPP homologs (24). The catalytic domain of KPP1 exhibits ~30% sequence identify to all of these *T. brucei* PPP homologs, but the N-terminal Plus3 domain in KPP1 is lacking from the *T. brucei* PPP homologs and is not found in any PPPs from any eukaryotic organisms except the kinetoplastid parasites, including *Trypanosoma cruzi* and *Leishmania* spp. (Figs. S1 and S2). Furthermore, despite the high sequence similarity of the catalytic domain of KPP1 to the PPPs, phylogenetic analysis using the catalytic domain places the KPP1 homologs in a distinct clade (Fig. S2*B*), similar to the results obtained using the full coding sequence (Fig. S2*A*). These results suggest that KPP1 is a unique member of the PPP family. Importantly, our data demonstrated that KPP1 is essential for *T. brucei* proliferation

(Fig. 3), suggesting that it can potentially be exploited as a drug target.

Although the mechanistic role of KPP1 remains to be elucidated, our results provided convincing evidence that KPP1 is necessary for proper positioning of the new flagellum and for maintenance of flagellum attachment. KPP1 localizes to multiple flagellum-associated cytoskeletal structures (Fig. 2), and depletion of KPP1 disrupts the duplication or segregation of these cytoskeletal structures that are required for positioning the flagellum and attachment of the flagellum to the cell body (Figs. 3–6). Notably, this pleiotropic defect is very similar to that caused by TbPLK RNAi (15) and excess expression of TbPLK by either ectopic overexpression (18) or stabilization due to failure in degradation (19). Unlike TbPLK overexpression, however, KPP1 overexpression does not cause any growth defect (data not shown), suggesting that the KPP1 protein level is not under tight control. Nevertheless, the essential involvement of KPP1 in flagellum positioning and attachment suggests that protein dephosphorylation carried out by KPP1 is as crucial as protein phosphorylation carried out by TbPLK in controlling this process in *T. brucei*. This point is corroborated by the previous finding that dephosphorylation of TbCentrin2 in the centrin arm is necessary for bilobe duplication, FAZ elongation, and flagellum attachment (17). Therefore, the lack of TbCentrin2 dephosphorylation in KPP1-deficient mitotic cells (Fig. 7) likely contributes, at least partly, to the defects observed in KPP1 RNAi cells.

The localization of KPP1 to different cytoskeletal structures at different cell-cycle stages suggests that KPP1 may dephosphorylate distinct substrates in these structures. This raises the question of how substrate specificity for KPP1 is determined. Substrate specificity of many protein phosphatases, exemplified by PP1 and PP2A, is determined by the large number of regulatory subunits, which target PP1 and PP2A to their substrates at different subcellular compartments (28). Other protein phosphatases, including PP2C and FCP/SCP (TFIIF-associating component of RNA polymerase II CTD phosphatase/small CTD phosphatase), contain both catalytic and regulatory domains in the same protein, and the regulatory domain may help determine substrate specificity, although how this is achieved remains poorly understood (28). The Plus3 domain in the N terminus of KPP1 is potentially involved in recognition of the phosphothreonine residue(s) in KPP1 substrates, as four of the five residues of the RTF1 Plus3 domain that are involved in recognition of the phosphothreonine residue of the human Spt5 protein (27) are conserved in KPP1 Plus3 domain (Fig. 1*B*, *blue arrowheads*). Given the potential antagonism of TbPLK by KPP1, we speculate that the candidate substrate(s) of KPP1 may be either TbPLK, which has multiple phosphothreonine sites including phosphor–Thr-198 in the T-loop (32), or TbPLK substrate(s) in the basal body, such as SPBB1, which has two phosphothreonine sites (8), or potential TbPLK substrate(s) at the new FAZ tip, such as CIF1/TOEFAZ1 (8, 33, 34), which has eight phosphothreonine sites (32), and TbSmee1 (35), which has three phosphothreonine sites (32). Future experiments are planned to investigate whether any of these proteins binds to the Plus3 domain of KPP1 and whether any of them is a substrate of KPP1.

Depletion of KPP1 caused accumulation of multinucleated (>2 nuclei) cells (Fig. 3*C*), indicative of defective cytokinesis, but a direct role for KPP1 in regulating cytokinesis remains to be determined. Multinucleated cells started to accumulate after 72 h of KPP1 RNAi induction, coincident with the accumulation of cells with detached flagella (Fig. 3*D*). Given that proper flagellum positioning and attachment are essential for cytokinesis in *T. burcei* (7, 12, 36, 37), it is difficult, if not impossible, to distinguish between the direct effect exerted by KPP1 RNAi and the indirect effect due to flagellum detachment. Nevertheless, KPP1 localizes to the distal tip of the new FAZ (Fig. 2), which constitutes the site from which cleavage furrow ingression is initiated (38), and 2N2K cells increased from ~11 to ~21% after KPP1 RNAi for 48 h, prior to massive flagellum detachment occurred (Fig. 3*C*), indicating that KPP1 likely also plays a direct role in cytokinesis.

In summary, we have identified a putative kinetoplastid-specific protein phosphatase, which plays essential roles in regulating the duplication and segregation of multiple flagellum-associated cytoskeletal structures to ensure proper positioning and attachment of the newly assembled flagellum. Our findings highlight the requirement of protein dephosphorylation in controlling flagellum inheritance, adding another layer of regulation to this process in addition to the previously discovered TbPLK-mediated protein phosphorylation.

Experimental procedures

Trypanosome cell culture

The procyclic *T. brucei* strain Lister 427 was cultured in SDM-79 medium supplemented with 10% heat-inactivated fetal bovine serum (Atlanta Biologicals, Inc.) at 27 °C. The Lister 427-derived 29-13 strain (39), which stably expresses the T7 RNA polymerase and the tetracycline repressor, was grown at 27 °C in SDM-79 medium containing 10% heat-inactivated fetal bovine serum, 15 μg/ml of G418, and 50 μg/ml of hygromycin B. Cells were routinely diluted with fresh medium when the cell density reached 5×10^6/ml.

RNAi

A 583-bp DNA fragment (nucleotide 993–1575) corresponding to the C-terminal portion of the *KPP1* coding sequence was PCR amplified (forward primer: 5′-ATCTAGCCCCTCGAGACAGTGTTCGGTGACATCCA-3′; reverse primer: 5′-TTCGATATCAAGCTTGCCCGAAGCCATATTTATCA-3′; underlined are XhoI and HindIII sites, respectively) and cloned into the pZJM vector (40). The resulting plasmid was linearized with NotI and electroporated into the 29-13 cell line. Transfectants were selected with 2.5 μg/ml of phleomycin and further cloned by limiting dilution in a 96-well plate containing the SDM-79 medium supplemented with 20% fetal bovine serum, 2.5 μg/ml of phleomycin, 15 μg/ml of G418, and 50 μg/ml of hygromycin B.

Epitope tagging of endogenous proteins

A 1,248-bp DNA fragment corresponding to the C-terminal coding sequence of KPP1 was PCR amplified (forward primer: 5′-GGCGAATTGGGTACCGTCGGTCAAAAGGGAATG-

ACG-3′; reverse primer: 5′-AGGATATTCCTTAAGAATGCGCTTAAGACGCGG-3′; underlined are KpnI and AflII sites, respectively) and cloned into the pC-3HA-PAC vector, which was derived from the pC-PTP-NEO vector (41) by replacing the PTP epitope with a triple HA epitope and the neomycin resistance gene (NEO) with the puromycin resistance gene (PAC). The resulting plasmid, pC-KPP1–3HA-PAC, was linearized with NcoI and transfected into the 427 cell line and the KPP1 RNAi cell line. Transfectants were selected with 1 μg/ml of puromycin and cloned by limiting dilution as described above.

Ectopic overexpression of WT and mutant KPP1 in T. brucei

The full-length coding sequence of KPP1 was PCR amplified from genomic DNA (forward primer: 5′-CATTCTTGACTCGAGATGGATCCACCTAATGTACCTCC-3′; reverse primer: 5′-AGGATATTCCTTAAGAATGCGCTTAAGACGCGG-3′, underlined are XhoI and AflII sites, respectively) and cloned into the pLew1000-3HA vector, which was modified from the pLew100 vector (39). Site-directed mutagenesis of Asp-371 to asparagine (D371N) and His-557 to lysine (H557K) in the active sites of KPP1 was carried out using the QuikChange II site-directed mutagenesis kit (Agilent, Inc.) using the following primers (D371N: forward primer, 5′-TTGTTCCTTGGCAACTATGTAGAT CGT-3′; reverse primer, 5′-ACGATCTACATAGTTGCCAAGGAACAA-3′; H557K: forward primer, 5′-TACATATTTCGTGCGTTTCAAGAAAAGGCGGAT-3′; reverse primer, 5′-ATCCGCCTTTTCTTGAAACGCACGAAATATGTA-3′). Mutation of the DNA sequences encoding the two residues was confirmed by sequencing. The pLew100-KPP1–3HA vector and the pLew100-KPP1$^{D371N\text{-}H557K}$-3HA vector were linearized with NotI and electroporated into the 29-13 cell line. Ectopic expression of WT and mutant KPP1 proteins was induced with 0.1 μg/ml of tetracycline for 16 h before being fixed for immunofluorescence microscopy.

Immunofluorescence microscopy

Control cells and KPP1 RNAi cells induced for 48 or 72 h were harvested by centrifugation, washed once with PBS, and then settled onto coverslips for 20 min at room temperature. Cells were immediately fixed with cold methanol at −20 °C for 30 min, rehydrated with PBS at room temperature for 10 min. After blocking with 3% BSA in PBS at room temperature for 30 min, cells were incubated with appropriate primary antibodies for 1 h at room temperature. The following primary antibodies were used: FITC-conjugated anti-HA mAb (1:400 dilution, Sigma), anti-TbPLK polyclonal antibody (1:1,000 dilution) (8), anti-LdCen1 polyclonal antibody (1:1,000 dilution) (42), anti-CC2D polyclonal antibody (1:2,000 dilution) (7), anti-TbSAS-6 polyclonal antibody (1:2,000 dilution) (43), L8C4 (anti-PFR2) mAb (1:50 dilution) (44), YL1/2 mAb (1:2,000 dilution, Millipore), L3B2 (anti-FAZ1) mAb (1:25 dilution) (44), 20H5 (anti-centrin) mAb (1:1,000 dilution, Millipore) (3), anti-TbBILBO1 polyclonal antibody (1:4,000 dilution) (45), anti-TbMORN1 polyclonal antibody (1:5,000 dilution) (31), and PS54 (anti-pSer-54 of TbCentrin2) polyclonal antibody (1:30,000 dilution) (17). After washing with PBS, cells were incubated with secondary antibodies for another 1 h at room temperature. The following secondary antibodies were used: Cy3-conjugated anti-rabbit IgG (1:400 dilution, Sigma), Cy3-conjugated anti-mouse IgG (1:400 dilution, Sigma), FITC-conjugated anti-rat IgG (1:400 dilution, Sigma), and FITC-conjugated anti-mouse IgG (1:400 dilution, Sigma). Cells were mounted with Vectashield mounting medium containing DAPI (Vector Labs), and visualized under an inverted fluorescence microscope (Olympus IX71) equipped with a cold CCD camera and a PlanApo N60X/1.42 immersion lens. Images were acquired with the Slidebook version 5.0 software.

Scanning electron microscopy

Scanning electron microscopic analysis of *T. brucei* cells was performed as described previously (23). To maintain cell shape and morphology, control cells and KPP1 RNAi cells induced for 72 h were washed once with PBS for 5 min at room temperature, and then fixed with 2.5% (v/v) glutaraldehyde for 2 h. Cells were washed three times with PBS, and settled on glass coverslips. After a brief washing with water, cells were dehydrated in alcohol (30, 50, 70, 90, and 100%, v/v) for 10 min in each solution. Samples were processed by critical point drying, and then coated with a 5-nm metal film (Pt:Pd 80:20, Ted Pella Inc.) using a sputter-coater (Cressington Sputter Coater 208 HR, Ted Pella Inc.). Cells were imaged under Nova NanoSEM 230 (FEI) using the following parameters: 5 mm for the scanning work distance and 8 kV for the accelerating high voltage.

Statistical analysis

Statistical analysis was performed using the *t* test in the Microsoft Excel software. Detailed *n* values for each panel in the figures were stated in the corresponding legends. For immunofluorescence microscopy, images were randomly taken and all cells in each image were counted.

Author contributions—Q. Z. and Z. L. conceptualization; Q. Z. validation; Q. Z., G. D., and Z. L. investigation; Q. Z. visualization; Q. Z. methodology; Q. Z. and Z. L. writing-original draft; Q. Z., G. D., and Z. L. writing-review and editing; G. D. software; G. D. and Z. L. formal analysis; Z. L. supervision; Z. L. funding acquisition; Z. L. project administration.

Acknowledgments—We thank Dr. Arthur Günzl for providing the epitope-tagging vector pC-PTP-NEO, Dr. Keith Gull for L3B2 (anti-FAZ1) and L8C4 (anti-PFR2) antibodies, Dr. Cynthia He for the anti-CC2D antibody, Dr. Hira Nakhashi for the anti-LdCen1 antibody, Dr. Christopher de Graffenried for the PS54 antibody, Dr. Derrick Robinson for the anti-BILBO1 antibody, and Dr. Brooke Morriswood for the anti-TbMORN1 antibody.

References

1. Gull, K. (1999) The cytoskeleton of trypanosomatid parasites. *Annu. Rev. Microbiol.* **53,** 629–655 CrossRef Medline
2. Briggs, L. J., McKean, P. G., Baines, A., Moreira-Leite, F., Davidge, J., Vaughan, S., and Gull, K. (2004) The flagella connector of *Trypanosoma brucei*: an unusual mobile transmembrane junction. *J. Cell Sci.* **117,** 1641–1651 CrossRef Medline
3. He, C. Y., Pypaert, M., and Warren, G. (2005) Golgi duplication in *Trypanosoma brucei* requires Centrin2. *Science* **310,** 1196–1198 CrossRef Medline

4. Kohl, L., Robinson, D., and Bastin, P. (2003) Novel roles for the flagellum in cell morphogenesis and cytokinesis of trypanosomes. *EMBO J.* **22,** 5336–5346 CrossRef Medline
5. Eliaz, D., Kannan, S., Shaked, H., Arvatz, G., Tkacz, I. D., Binder, L., Waldman Ben-Asher, H., Okalang, U., Chikne, V., Cohen-Chalamish, S., and Michaeli, S. (2017) Exosome secretion affects social motility in *Trypanosoma brucei*. *PLoS Pathog.* **13,** e1006245 CrossRef
6. Imhof, S., Fragoso, C., Hemphill, A., von Schubert, C., Li, D., Legant, W., Betzig, E., and Roditi, I. (2016) Flagellar membrane fusion and protein exchange in trypanosomes; a new form of cell-cell communication? *F1000Res* **5,** 682 CrossRef Medline
7. Zhou, Q., Liu, B., Sun, Y., and He, C. Y. (2011) A coiled-coil- and C2-domain-containing protein is required for FAZ assembly and cell morphology in *Trypanosoma brucei*. *J. Cell Sci.* **124,** 3848–3858 CrossRef
8. Hu, H., Zhou, Q., and Li, Z. (2015) A novel basal body protein that is a Polo-like kinase substrate is required for basal body segregation and flagellum adhesion in *Trypanosoma brucei*. *J. Biol. Chem.* **290,** 25012–25022 Medline
9. Morgan, G. W., Denny, P. W., Vaughan, S., Goulding, D., Jeffries, T. R., Smith, D. F., Gull, K., and Field, M. C. (2005) An evolutionarily conserved coiled-coil protein implicated in polycystic kidney disease is involved in basal body duplication and flagellar biogenesis in *Trypanosoma brucei*. *Mol. Cell. Biol.* **25,** 3774–3783 CrossRef
10. Absalon, S., Kohl, L., Branche, C., Blisnick, T., Toutirais, G., Rusconi, F., Cosson, J., Bonhivers, M., Robinson, D., and Bastin, P. (2007) Basal body positioning is controlled by flagellum formation in *Trypanosoma brucei*. *PLoS ONE* **2,** e437 CrossRef
11. Zhou, Q., Gheiratmand, L., Chen, Y., Lim, T. K., Zhang, J., Li, S., Xia, N., Liu, B., Lin, Q., and He, C. Y. (2010) A comparative proteomic analysis reveals a new bi-lobe protein required for bi-lobe duplication and cell division in *Trypanosoma brucei*. *PLoS ONE* **5,** e9660 CrossRef
12. Vaughan, S., Kohl, L., Ngai, I., Wheeler, R. J., and Gull, K. (2008) A repetitive protein essential for the flagellum attachment zone filament structure and function in *Trypanosoma brucei*. *Protist* **159,** 127–136
13. Umeyama, T., and Wang, C. C. (2008) Polo-like kinase is expressed in $S/G_2/M$ phase and associated with the flagellum attachment zone in both procyclic and bloodstream forms of *Trypanosoma brucei*. *Eukaryot. Cell* **7,** 1582–1590 CrossRef
14. de Graffenried, C. L., Ho, H. H., and Warren, G. (2008) Polo-like kinase is required for Golgi and bilobe biogenesis in *Trypanosoma brucei*. *J. Cell Biol.* **181,** 431–438 CrossRef Medline
15. Ikeda, K. N., and de Graffenried, C. L. (2012) Polo-like kinase is necessary for flagellum inheritance in *Trypanosoma brucei*. *J. Cell Sci.* **125,** 3173–3184 CrossRef
16. Yu, Z., Liu, Y., and Li, Z. (2012) Structure-function relationship of the Polo-like kinase in *Trypanosoma brucei*. *J. Cell Sci.* **125,** 1519–1530 CrossRef Medline
17. de Graffenried, C. L., Anrather, D., Von Raußendorf, F., and Warren, G. (2013) Polo-like kinase phosphorylation of bilobe-resident TbCentrin2 facilitates flagellar inheritance in *Trypanosoma brucei*. *Mol. Biol. Cell* **24,** 1947–1963 CrossRef Medline
18. Hammarton, T. C., Kramer, S., Tetley, L., Boshart, M., and Mottram, J. C. (2007) *Trypanosoma brucei* Polo-like kinase is essential for basal body duplication, kDNA segregation and cytokinesis. *Mol. Microbiol.* **65,** 1229–1248 CrossRef Medline
19. Hu, H., Zhou, Q., Han, X., and Li, Z. (2017) $CRL4^{WDR1}$ controls Polo-like kinase protein abundance to promote bilobe duplication, basal body segregation and flagellum attachment in *Trypanosoma brucei*. *PLoS Pathog.* **13,** e1006146 CrossRef Medline
20. Hunter, T. (1995) Protein kinases and phosphatases: the yin and yang of protein phosphorylation and signaling. *Cell* **80,** 225–236 CrossRef Medline
21. Yamashiro, S., Yamakita, Y., Totsukawa, G., Goto, H., Kaibuchi, K., Ito, M., Hartshorne, D. J., and Matsumura, F. (2008) Myosin phosphatase-targeting subunit 1 regulates mitosis by antagonizing polo-like kinase 1. *Dev. Cell* **14,** 787–797 CrossRef Medline
22. Foley, E. A., Maldonado, M., and Kapoor, T. M. (2011) Formation of stable attachments between kinetochores and microtubules depends on the B56-PP2A phosphatase. *Nat. Cell. Biol.* **13,** 1265–1271 CrossRef Medline
23. Zhou, Q., Hu, H., and Li, Z. (2016) An EF-hand-containing protein in *Trypanosoma brucei* regulates cytokinesis initiation by maintaining the stability of the cytokinesis initiation factor CIF1. *J. Biol. Chem.* **291,** 14395–14409 CrossRef Medline
24. Szöör, B. (2010) Trypanosomatid protein phosphatases. *Mol. Biochem. Parasitol.* **173,** 53–63 CrossRef Medline
25. Arnold, K., Bordoli, L., Kopp, J., and Schwede, T. (2006) The SWISS-MODEL workspace: a web-based environment for protein structure homology modelling. *Bioinformatics* **22,** 195–201 CrossRef Medline
26. de Jong, R. N., Truffault, V., Diercks, T., Ab, E., Daniels, M. A., Kaptein, R., and Folkers, G. E. (2008) Structure and DNA binding of the human Rtf1 Plus3 domain. *Structure* **16,** 149–159 CrossRef Medline
27. Wier, A. D., Mayekar, M. K., Héroux, A., Arndt, K. M., and VanDemark, A. P. (2013) Structural basis for Spt5-mediated recruitment of the Paf1 complex to chromatin. *Proc. Natl. Acad. Sci. U.S.A.* **110,** 17290–17295 CrossRef Medline
28. Shi, Y. (2009) Serine/threonine phosphatases: mechanism through structure. *Cell* **139,** 468–484 CrossRef Medline
29. Robinson, D. R., and Gull, K. (1991) Basal body movements as a mechanism for mitochondrial genome segregation in the trypanosome cell cycle. *Nature* **352,** 731–733 CrossRef Medline
30. Shi, J., Franklin, J. B., Yelinek, J. T., Ebersberger, I., Warren, G., and He, C. Y. (2008) Centrin4 coordinates cell and nuclear division in *T. brucei*. *J. Cell Sci.* **121,** 3062–3070 CrossRef Medline
31. Morriswood, B., He, C. Y., Sealey-Cardona, M., Yelinek, J., Pypaert, M., and Warren, G. (2009) The bilobe structure of *Trypanosoma brucei* contains a MORN-repeat protein. *Mol. Biochem. Parasitol.* **167,** 95–103 CrossRef Medline
32. Urbaniak, M. D., Martin, D. M., and Ferguson, M. A. (2013) Global quantitative SILAC phosphoproteomics reveals differential phosphorylation is widespread between the procyclic and bloodstream form lifecycle stages of *Trypanosoma brucei*. *J. Proteome Res.* **12,** 2233–2244 CrossRef
33. Zhou, Q., Gu, J., Lun, Z. R., Ayala, F. J., and Li, Z. (2016) Two distinct cytokinesis pathways drive trypanosome cell division initiation from opposite cell ends. *Proc. Natl. Acad. Sci. U.S.A.* **113,** 3287–3292 CrossRef Medline
34. McAllaster, M. R., Ikeda, K. N., Lozano-Núñez, A., Anrather, D., Unterwurzacher, V., Gossenreiter, T., Perry, J. A., Crickley, R., Mercadante, C. J., Vaughan, S., and de Graffenried, C. L. (2015) Proteomic identification of novel cytoskeletal proteins associated with TbPLK, an essential regulator of cell morphogenesis in *Trypanosoma brucei*. *Mol. Biol. Cell* **26,** 3013–3029 CrossRef Medline
35. Perry, J. A., Sinclair-Davis, A. N., McAllaster, M. R., and de Graffenried, C. L. (2018) TbSmee1 regulates hook complex morphology and the rate of flagellar pocket uptake in *Trypanosoma brucei*. *Mol. Microbiol.* **107,** 344–362 CrossRef
36. Zhou, Q., Hu, H., He, C. Y., and Li, Z. (2015) Assembly and maintenance of the flagellum attachment zone filament in *Trypanosoma brucei*. *J. Cell Sci.* **128,** 2361–2372 CrossRef Medline
37. Moreira, B. P., Fonseca, C. K., Hammarton, T. C., and Baqui, M. M. (2017) Giant FAZ10 is required for flagellum attachment zone stabilization and furrow positioning in *Trypanosoma brucei*. *J. Cell Sci.* **130,** 1179–1193 Medline
38. Vaughan, S., and Gull, K. (2008) The structural mechanics of cell division in *Trypanosoma brucei*. *Biochem. Soc. Trans.* **36,** 421–424 CrossRef
39. Wirtz, E., Leal, S., Ochatt, C., and Cross, G. A. (1999) A tightly regulated inducible expression system for conditional gene knock-outs and dominant-negative genetics in *Trypanosoma brucei*. *Mol. Biochem. Parasitol.* **99,** 89–101 CrossRef
40. Wang, Z., Morris, J. C., Drew, M. E., and Englund, P. T. (2000) Inhibition of *Trypanosoma brucei* gene expression by RNA interference using an integratable vector with opposing T7 promoters. *J. Biol. Chem.* **275,** 40174–40179 CrossRef Medline
41. Schimanski, B., Nguyen, T. N., and Güunzl, A. (2005) Highly efficient tandem affinity purification of trypanosome protein complexes based on a

novel epitope combination. *Eukaryot. Cell* **4,** 1942–1950 CrossRef Medline

42. Selvapandiyan, A., Kumar, P., Morris, J. C., Salisbury, J. L., Wang, C. C., and Nakhasi, H. L. (2007) Centrin1 is required for organelle segregation and cytokinesis in *Trypanosoma brucei*. *Mol. Biol. Cell* **18,** 3290–3301 CrossRef
43. Hu, H., Liu, Y., Zhou, Q., Siegel, S., and Li, Z. (2015) The centriole cartwheel protein SAS-6 in *Trypanosoma brucei* is required for probasal body biogenesis and flagellum assembly. *Eukaryot. Cell* **14,** 898–907 CrossRef Medline
44. Kohl, L., Sherwin, T., and Gull, K. (1999) Assembly of the paraflagellar rod and the flagellum attachment zone complex during the *Trypanosoma brucei* cell cycle. *J. Eukaryot. Microbiol.* **46,** 105–109 CrossRef Medline
45. Bonhivers, M., Nowacki, S., Landrein, N., and Robinson, D. R. (2008) Biogenesis of the trypanosome endo-exocytotic organelle is cytoskeleton mediated. *PLos Biol.* **6,** e105 CrossRef Medline